Molecular Dynamics Simulations of Small *n*-Alkane Clusters in a Mesoscopic Solvent

Seo Young Ko and Song Hi Lee*

Department of Chemistry, Kyungsung University, Pusan 608-736, Korea
Received February 28, 2003

The structural and dynamic properties of small *n*-alkane clusters embedded in a mesoscopic solvent are investigated. The solvent interactions are taken into account through a multi-particle collision operator that conserves mass, momentum and energy and the solvent dynamics is updated at discrete time intervals. The cluster molecules interact among themselves and with the solvent molecules through intermolecular forces. The properties of *n*-heptane and *n*-decane clusters interacting with the mesoscopic solvent molecules through repulsive Lennard-Jones interactions are studied as a function of the number of the mesoscopic solvent molecules. Modifications of both the cluster and solvent structure as a result of cluster-solvent interactions are considered. The cluster-solvent interactions also affect the dynamics of the small *n*-alkane clusters.

Key Words : Molecular dynamics simulation, Mesoscopic solvent, *n*-Alkane clusters

Introduction

It is often useful to focus on the dynamics of a subsystem of interest and treat the rest of the system at a less detailed level of description. The classical theories of Brownian motion recognized this distinction and reduced the influence of the solvent on the Brownian particles to friction forces and random forces with simple statistical properties.[1] In many applications such a simplified description is not sufficient since one would like to account for specific features of the solute-solvent force. In other words, one is interested in the detailed microscopic dynamics of some degrees of freedom of the system interacting with a solvent whose dynamics is essential for the phenomena but whose detailed properties are not interest. The systems are sufficiently complex that a full molecular dynamics (MD) simulation of the system plus solvent is impossible.

In such circumstances one is led to consider mesoscopic models for the solvent dynamics that incorporate the essential dynamical properties, yet are simple enough to be simulated for long times and on long distance scales.[2] A variety of mesoscopic models have been constructed for this purpose ranging from Langevin models that have been employed as simple "heat baths" in MD studies of biomolecule dynamics,[3] to schemes such as Direct Simulation Monte Carlo (DSMC) methods,[4] lattice Boltzmann methods,[5] and extensions of hydrodynamic lattice gas automaton models.[6]

Recently Kapral and co-workers have reported results of a mesoscopic model for solvent dynamics,[7] solute molecular dynamics in a mesoscale solvent,[8] and cluster structure and dynamics in a mesoscopic solvent.[9] In this model, fluid particles interact through multi-particle collision events which take place at discrete time intervals. Between such collision events the particles undergo free streaming motion. The dynamics conserves mass, momentum, and energy and yields the exact hydrodynamic equations of motion for the conserved fields on long distance and time scales. One may consider the dynamics of solute molecules in this mesoscopic solvent and because the solvent is described at an effective particle level the solute and solvent molecules interact through intermolecular forces rather than through boundary conditions. This leads to a hybrid description of the dynamics where solute molecules evolve by Newton's equations of motion but the solvent evolves through the multi-particle mesoscale dynamics.

In the present paper, we carry out molecular dynamic (MD) simulations of *n*-alkane clusters with numbers of 100 molecules in order to investigate the structure and dynamics of complex molecular entities in the mesoscopic solvent. Conditions are chosen so that the clusters persist in vacuum in liquid-like states for long time periods without evaporation. We then study the modifications in the cluster structure and dynamics when they are embedded in the mesoscopic solvent. The number of the mesoscopic solvent molecules is varied to investigate how the cluster properties change.

This paper is organized as follows: In Section II, we present the molecular models and MD simulation methods. We discuss our simulation results in Section III and present concluding remarks in Section IV.

Molecular Models and MD Simulation Methods

The system we investigate comprises a cluster, whose molecules interact through attractive intermolecular forces, embedded in a solvent whose dynamics is treated at a mesoscopic level. The solvent molecules labeled 1, $\cdots, N$ have phase space coordinates $(\boldsymbol{r}^{(N)}, \boldsymbol{v}^{(N)}) = (\boldsymbol{r}_1, \boldsymbol{r}_2, \cdots, \boldsymbol{r}_N, \boldsymbol{v}_1, \boldsymbol{v}_2, \cdots, \boldsymbol{v}_N)$, while the cluster molecules, labeled $N+1, \cdots, N+M$ have phase space coordinates $(\boldsymbol{r}^{(M)}, \boldsymbol{v}^{(M)}) = (\boldsymbol{r}_{N+1}, \boldsymbol{r}_{N+2}, \cdots, \boldsymbol{r}_{N+M}, \boldsymbol{v}_{N+1}, \boldsymbol{v}_{N+2}, \cdots, \boldsymbol{v}_{N+M})$.

The total potential energy of the system is made up of cluster molecule-cluster molecule and cluster molecule-solvent molecule interactions,

$$V(\boldsymbol{r}^{(M)}, \boldsymbol{r}^{(N)}) = V_{cc}(\boldsymbol{r}^{(M)}) + V_{cs}(\boldsymbol{r}^{(M)}, \boldsymbol{r}^{(N)}). \quad (1)$$

*Corresponding author. E-mail: shlee@star.ks.ac.kr

There are no solvent molecule-solvent molecule interactions since these are taken into account by multi-particle collisions in the mesoscopic treatment of the solvent dynamics. To carry out multi-particle solvent molecule collisions, the system is partitioned into cells and time is divided into discrete time intervals τ. At any time instant, a cell will contain a certain number of solvent molecules. At the discrete time instants, the solvent molecules undergo multi-particle collisions which are carried out in the following way: each cell is assigned at random a rotation operator ω from a set of rotation operators, Ω. The velocity of each solvent molecule in the cell is rotated relative to the center of mass velocity of the molecules in the cell $\boldsymbol{V}$ by the rotation operator $\hat{\omega}$,

$$\boldsymbol{v}_i \rightarrow \boldsymbol{V} + \hat{\omega}[\boldsymbol{v}_i - \boldsymbol{V}]. \tag{2}$$

Such multi-particle collisions are carried out independently in each cell.

For times between the discrete time intervals at which solvent multi-particle collisions take place, all particles in the system, cluster molecules and solvent molecules, evolve according to Newton's equations of motion,

$$\dot{\boldsymbol{r}}_i = \boldsymbol{v}_i,$$
$$m_i \dot{\boldsymbol{v}}_i = -\frac{\partial V}{\partial \boldsymbol{r}_i} = \boldsymbol{F}_i, \tag{3}$$

where m_i is the mass of particle i and the potential energy V is that given in Eq. (1). If the solvent molecules are within the range of interaction of the solvent-cluster potential energy, then their dynamics is influenced by these interactions; otherwise they simply undergo free streaming motion.

Given the above description of the model, the system Hamiltonian is

$$H = \sum_i \frac{1}{2} m_i \boldsymbol{v}_i^2 + \sum_{i<j} V_{ij}(|\boldsymbol{r}_i - \boldsymbol{r}_j|), \tag{4}$$

where i = c if i is a cluster molecule and s if it is a solvent molecule. The cluster molecules interact with each other via Lennard-Jones (LJ) potentials,

$$V_{cc} = 4\varepsilon_{cc}\left[\left(\frac{\sigma_{cc}}{r}\right)^{12} - \left(\frac{\sigma_{cc}}{r}\right)^{6}\right], \tag{5}$$

while the cluster molecule-solvent molecule interactions are repulsive and are given by truncated LJ potentials,

$$V_{cs} = \begin{cases} 4\varepsilon_{cs}\left[\left(\frac{\sigma_{cs}}{r}\right)^{12} - \left(\frac{\sigma_{cs}}{r}\right)^{6} + \frac{1}{4}\right], & r \le 2^{1/6}\sigma_{cs} \\ 0, & r > 2^{1/6}\sigma_{cs} \end{cases}. \tag{6}$$

We used a united atom (UA) model for *n*-alkanes, that is, methyl and methylene groups are considered as spherical interaction sites centered at each carbon atom. This model was used in the previous simulation studies.[10-17] Here, we briefly describe the salient features of the model. The interaction between the sites on different *n*-alkane molecules and between the sites separated by more than three bonds in the same *n*-alkane molecule was described by a Lennard-Jones (LJ) potential. All the sites in a chain have the same LJ size parameter $\sigma_i \equiv \sigma_{ii}$ = 3.93 A, and the well depth parameters were $\varepsilon_i \equiv \varepsilon_{ii}$ = 0.9498 kJ/mol for interactions between the end sites and ε_i = 0.3891 kJ/mol for interactions between the internal sites. The Lorentz-Berthelot combining rules [$\varepsilon_{ij} \equiv (\varepsilon_i\varepsilon_j)^{1/2}$, $\sigma_{ij} \equiv (\sigma_i + \sigma_j)/2$] were used for interactions between an end site and an internal site. A cut-off distance of 2.5 σ_i was used for all the LJ interactions.

The bond-stretching interaction was ignored by a constraint force which keeps intramolecular nearest neighbors at a fixed distance. The bond-angle bending interaction was described by a harmonic potential with an equilibrium angle of 114° and a force constant of 0.07920 kJ/mol/degree^2. The torsional interaction was described by the potential developed by Jorgensen *et al.*[18]:

$$U_{torsion}(\phi) = a_0 + a_1\cos\phi + a_2\cos^2\phi + a_3\cos^3\phi \tag{7}$$

where ϕ is the dihedral angle, and a_0 = 8.3973 kJ/mol, a_1 = 16.7862 kJ/mol, a_2 = 1.1339 kJ/mol, and a_3 = –26.3174 kJ/mol.

The mesoscopic solvent molecule was modeled for a methane molecule with mass of m_s = 16.043 g/mol and the LJ parameters of σ_{cs} = 3.93 A and ε_{cs} = 0.9967 and 0.6380 kJ/mol for interactions with the end sites and the internal sites of *n*-alkane molecules in Eq. (6).

For *n*-alkanes, we have chosen 2 systems - *n*-heptane (C_7H_{16}) and *n*-decane($C_{10}H_{22}$). First, each MD simulation was carried out in vacuum and examined which temperature the *n*-alkane cluster exists in the liquid state and persists with no evaporation during 2-5 ns of our simulations for the given LJ parameters. Then, at the determined temperature for each vacuum cluster, the usual MD simulation with the periodic boundary condition in the x-, y-, and z-directions and the minimum image convention for pair potential was carried out in the NpT ensemble to determine the density of the system of p = 1 atm, and was continued in the NVT ensemble. The number of *n*-alkane was M = 100, the density and hence the length of cubic simulation box were fixed and listed in Table 1 with given temperatures. Newton's equations of motion were integrated using the velocity Verlet algorithm[19] with a time step of Δt = 0.002 ps. RATTLE algorithm[20] was used for the constraint of the fixed C-C bond length. Gaussian isokinetics was used to keep the temperature of the system constant.[21,22]

The cluster simulations were carried out in a cubic box of length L = 54.4 A with periodic boundary conditions containing N = 2,000, 4,000, 8,000, 16,000, or 32,000 solvent molecules. To perform multi-particle solvent collisions, the simulation box was divided into $(6)^3$, $(8)^3$, $(10)^3$, or $(14)^3$ cells according to the number of solvent molecules, N. The typical number density of solvent molecules in a cell is 10,[7-9] but it was

Table 1. MD simulation parameters for molecular models of *n*-alkanes

n-alkanes	number of *n*-alkanes	mass of site (g/mole)	T (K)	density (g/cc)	length of box (A)
n-C_7H_{16}	100	14.315	170.0	0.8379	27.08
n-$C_{10}H_{22}$	100	14.2286	190.0	0.8246	30.60

verified by our MD simulations that a minor variation of the number density does not affect the structural and dynamic properties of the *n*-alkane clusters and the mesoscopic solvent. Multi-particle solvent collisions were carried out every 50 molecular dynamics time steps so that $\tau = 0.1$ ps. At these discrete time intervals, the velocities of all solvent molecules in a frame moving with the velocity of the center of mass of the particles in each cell were rotated by $\pi/2$ along a randomly chosen direction independently in each cell. After a total of 2,000,000 time steps (4.0 ns) for equilibration, the equilibrium properties were then averaged over 5 blocks of 500,000 time steps (1.0 ns).

Results and Discussion

Thermodynamic and Structural Properties. Some equilibrium properties for *n*-alkane clusters of M = 100 in vacuum and in the mesoscopic solvents obtained from our MD simulations are listed in Tables 2 and 3. The total Lennard-Jones (LJ) energy between C-C sites of *n*-alkane increases roughly with the number of the mesoscopic solvent molecules, N, since the mesoscopic solvent puts the squeeze on the cluster, but it decreases when N is too large. However, the intra LJ energy within the same *n*-alkane chain decreases with increasing N and increases when N is too large. This is coincided with the increase of C-C-C-C *trans* % and the decrease of torsional energy with increasing N. The squeeze of the mesoscopic solvent on the cluster is easily seen from the cluster-solvent repulsion LJ interaction energy which increases proportionally to N. In the cases of both *n*-alkane clusters, the chain backbone tends to straighten up and then bend down upon the squeeze of the mesoscopic solvent, which one might misunderstood as it bends down continually.

The calculated square radii of gyration (R_g^2) and the square end-to-end distances (R_{ee}^2) of both *n*-alkane clusters show the same trend, increase with increasing N but decrease when N is too large. As N increases, there is a reduction in the degree of symmetry for *n*-heptane, followed by an augmentation when N = 16,000 and 32,000, as shown by an increase of the largest eigenvalues (l_1^2) of the mass tensor listed in Table 2. l_1 corresponds to the smallest eigenvalue of the inertia tensor and the associated eigenvector defines the direction of the longest principal axis of the molecule's ellipsoid of inertia.[23] These eigenvalues (l_i^2) satisfy the relation $l_1^2 + l_2^2 + l_3^2 = R_g^2$ with $l_1^2 > l_2^2 > l_3^2$. The second largest eigenvalues (l_2^2) of the mass tensor decreases with increasing N and increases when N = 16,000 and 32,000, compensating for the change of l_i^2. The turnover seems to occur at N = 16,000 for the *n*-heptane cluster and at N = 8,000 for the *n*-decane cluster, respectively.

It is convenient to characterize the cluster structure in terms of the site radial distribution functions for cluster and solvent molecules relative to the cluster center of mass. These distribution functions are defined by

$$g_{CM-\alpha}(r) = \frac{1}{4\pi r^2 \rho_\alpha}\left[\sum_i^{N_\alpha} \delta(|\boldsymbol{r}_i - \boldsymbol{R}_{CM}| - r)\right] \qquad (7)$$

Table 2. Thermodynamic and static properties of *n*-heptane clusters in vacuum and in the mesoscopic solvents at 170 K. Uncertainties in the last reported digit(s) are given in parenthesis

Properties	Vacuum	N = 2,000	N = 4,000	N = 8,000	N = 16,000	N = 32,000
total LJ energy[a]	−28.32(3)	−29.83(5)	−31.35(26)	−34.11(24)	−33.91(7)	−32.41(20)
intra LJ energy	−1.575(20)	−1.557(9)	−1.520(18)	−1.405(6)	−1.430(7)	−1.566(13)
cluster-solvent E.	–	35.82(4)	71.31(5)	141.0(4)	279.9(5)	555.4(2)
torsional energy	1.235(36)	1.184(15)	1.099(32)	0.856(22)	0.905(12)	1.155(47)
trans %	86.40(18)	87.44(15)	89.48(17)	95.38(13)	93.95(14)	87.63(23)
R_g^2 (A^2)	6.37(3)	6.40(1)	6.47(3)	6.66(2)	6.61(11)	6.38(3)
R_{ee}^2 (A^2)	53.53(45)	53.97(22)	54.87(34)	57.59(27)	56.92(22)	53.97(21)
l_1^2/R_g^2 (%)	94.61(22)	94.85(10)	95.24(20)	96.49(11)	96.20(9)	94.88(15)
l_2^2/R_g^2 (%)	4.66(17)	4.47(7)	4.17(17)	3.17(9)	3.40(8)	4.43(12)

[a]In kJ/mol.

Table 3. Thermodynamic and static properties of *n*-decane clusters in vacuum and in the mesoscopic solvents at 190 K. Uncertainties in the last reported digit(s) are given in parenthesis

Properties	Vacuum	N = 2,000	N = 4,000	N = 8,000	N = 16,000	N = 32,000
total LJ energy[a]	–45.45(13)	–47.75(9)	–48.14(41)	–48.59(13)	–47.31(71)	–44.26(28)
intra LJ energy	–2.587(18)	–2.500(6)	–2.485(17)	–2.493(11)	–2.677(26)	–3.081(10)
cluster-solvent E.	–	47.23(2)	94.71(35)	188.2(2)	372.4(8)	729.3(3)
torsional energy	0.959(17)	0.849(7)	0.830(19)	0.819(12)	0.984(33)	1.398(22)
trans %	94.87(13)	97.09(13)	97.43(15)	97.47(11)	93.50(34)	84.05(19)
R_g^2 (A^2)	13.34(4)	13.56(1)	13.60(4)	13.58(3)	13.17(3)	12.18(2)
R_{ee}^2 (A^2)	126.7(7)	130.1(0)	130.7(6)	130.4(4)	124.2(5)	109.5(4)
l_1^2/R_g^2 (%)	97.39(13)	98.01(0)	98.13(9)	98.02(8)	96.98(20)	94.28(9)
l_2^2/R_g^2 (%)	2.25(11)	1.73(1)	1.62(8)	1.73(7)	2.61(17)	4.89(13)

[a]In kJ/mol.

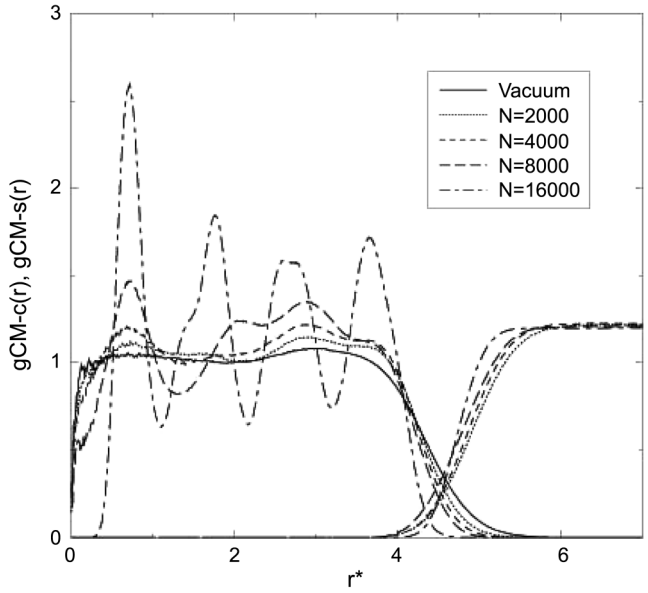

Figure 1. Site radial distribution functions $g_{CM-c}(r)$ and $g_{CM-s}(r)$ versus $r^*(= r/\sigma)$ for *n*-heptane clusters of M = 100 in vacuum and in the mesoscopic solvents.

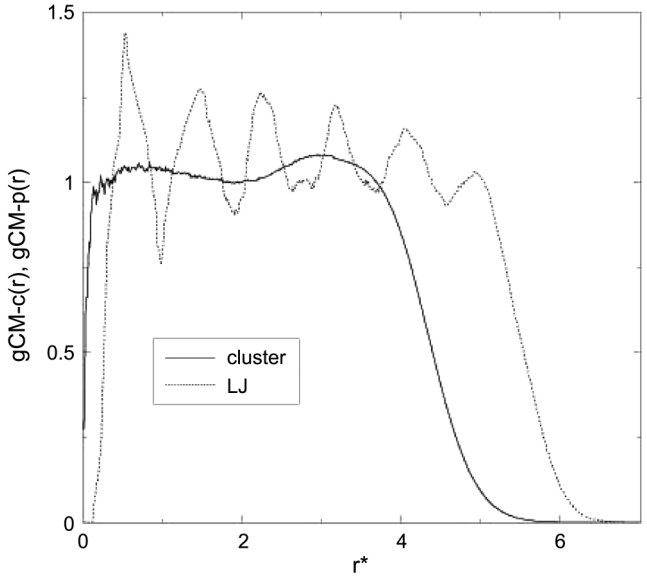

Figure 2. Comparison of site radial distribution function $g_{CM-c}(r)$ for *n*-heptane clusters of M = 100 in vacuum with site radial distribution function $g_{CM-P}(r)$ for Lennard-Jones particles of M = 700 in vacuum.

where a = c or s designates a site of cluster molecule or solvent molecule, $\boldsymbol{R}_{CM}$ is the center of mass of the cluster and ρ_a is the number density of sites of cluster or solvent molecules. In this expression, $\rho_c = M/(4\pi R^3/3)$, where R is the radius of cluster (15.7 A and 18.1 A for *n*-heptane and *n*-decane, respectively), and $\rho_s = nN/(54.4\ \text{A})^3$ with n the number of sites in *n*-alkane.

Figure 1 shows the site radial distribution function for *n*-heptane clusters of M = 100 in vacuum and in the mesoscopic solvents at T = 170 K. The graph of $g_{CM-c}(r)$ in vacuum shows liquid-like distributions of cluster particles and no structural ordering within the cluster. No prominent cluster particle layer is seen in the *n*-heptane clusters in vacuum at T = 170 K. The previous study for Lennard-Jones (LJ) clusters of M = 25 and 123 in a mesoscopic solvent[9] reported two and three prominent cluster particle layers, respectively, within liquid-like distributions of cluster particles. The structural feature of the site radial distribution function for *n*-heptane clusters in vacuum is originated in two facts - the vivid movement of cluster molecules and the connection of sites in the *n*-heptane chain backbone. First we have verified the liquid-like character of cluster by computing the mean-square displacement of the cluster molecules.

Second we have carried out an MD simulation of 700 LJ particles in vacuum at 170 K with four times strong ε to prevent from evaporation and the same σ. Figure 2 compares the resulting radial distribution function $g_{CM-P}(r)$ for LJ particles in vacuum with $g_{CM-c}(r)$ for *n*-heptane clusters in vacuum. The graph of $g_{CM-P}(r)$ shows liquid-like distribution of LJ particles with six prominent cluster particle layers, while that of $g_{CM-c}(r)$ is much compact due to the connection of sites in the *n*-heptane chain backbone and the interactions between the *n*-heptane chains.

Next, we consider the modifications in the cluster structure that occur when the clusters are embedded in the mesoscopic solvent. Since the solvent interacts with the cluster particles through the repulsive LJ interaction, we can study the modifications in the cluster structure and dynamics as a function of the number of the mesoscopic solvent molecules, N. In the cases of N = 2,000 and 4,000 the structures of the radial distribution functions are similar to the corresponding vacuum structure. As N increases, prominent cluster particle layers become appeared and four prominent cluster particle layers are clearly seen when N = 16,000. This might mislead the cluster structure of N = 16,000 as a solid-like configuration but the liquid-like character of the cluster is verified by computing the mean-square displacement of the cluster molecules.

Also, in Figure 1 we show the radial distribution functions $g_{CM-s}(r)$ for the solvent molecules relative to the cluster center of mass. As N increases, this radial distribution function becomes a solid well. The origin of the structural differences of the *n*-heptane clusters in N = 2,000 and in N = 1,6000 can be found in the structure of the solvent molecule-cluster particle distributions. Since the solvent molecules are not able to penetrate into the cluster due to the cluster-solvent repulsion LJ interaction, the solvent of N = 16,000 provides a larger external force on the cluster which compresses it and induces a prominent cluster particle layer configuration. The values of $g_{CM-s}(r)$ for both *n*-alkane clusters at large r^* are greater than unity because the cluster molecules exclude the solvent molecules around the center of system.

The results presented in Figure 3 for $g_{CM-c}(r)$ and $g_{CM-s}(r)$ for *n*-decane clusters of M = 100 in vacuum and in the mesoscopic solvents at T = 190 K exhibit structural changes similar to those for the *n*-heptane clusters of M = 100. Again, the graph of $g_{CM-c}(r)$ in vacuum shows liquid-like distributions of cluster particles and no prominent cluster

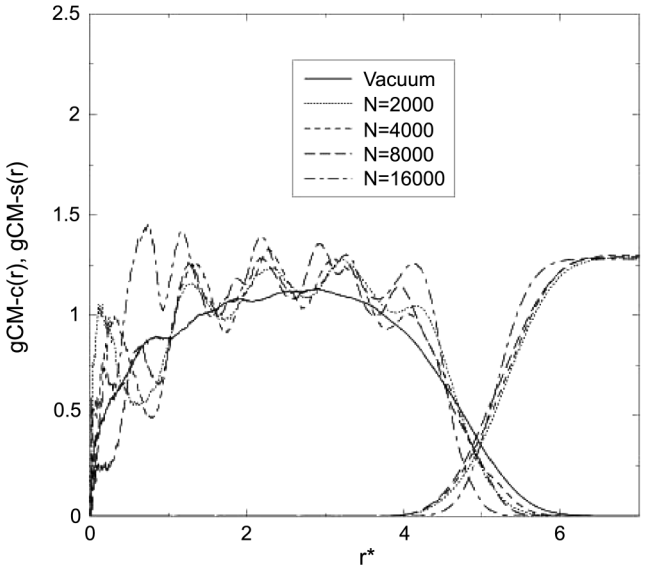

Figure 3. Site radial distribution functions $g_{CM-c}(r)$ and $g_{CM-s}(r)$ versus r^* (= r/σ) for *n*-decane clusters of M = 100 in vacuum and in the mesoscopic solvents.

particle layer is seen in the *n*-decane clusters in vacuum at T = 190 K. However, no clear difference of $g_{CM-c}(r)$ for the *n*-decane clusters in the mesocopic solvents with different N can be found except the case of N = 16,000 in which four prominent cluster particle layers are seen.

Cluster Diffusion. The vacuum clusters were prepared with no net translation of the center of mass of the cluster. However, in the presence of the solvent, the cluster as a whole may diffuse and this diffusion provides information on the interactions of the cluster with its environment.

There are two routes to determine self-diffusion constants from MD simulation; the Einstein relation from the mean square displacement (MSD),[24]

$$D_{self} = \frac{1}{6}\lim_{t\to\infty}\frac{d\langle|\boldsymbol{r}(t)-\boldsymbol{r}(0)|\rangle^2}{dt}, \tag{8}$$

and the Green-Kubo relation from the velocity autocorrelation (VAC) function,[24]

$$D_{self} = \frac{1}{3}\int_0^\infty \langle \boldsymbol{v}_i(t)\cdot\boldsymbol{v}_i(0)\rangle dt. \tag{9}$$

Self-diffusion constants of the center of mass for *n*-alkane clusters of M = 100 in the mesoscopic solvents, D_{CM}, obtained from both the Einstein relation, Eq. (8), and the Green-Kubo relation, Eq. (9), were collected in Table 4. First of all, the self-diffusion coefficients extracted from these two relations are in good agreement.

The value of D_{CM} of the center of mass for the *n*-alkane cluster in the mesoscopic solvent decreases with increasing N, which is fully understood by the structure of the solvent molecule-cluster particle distributions. As N increases, the cluster-solvent repulsion LJ interaction energy increases proportionally to N and the mesoscopic solvent puts the squeeze on the cluster increasingly. This restricts the diffusion of *n*-alkane clusters more.

The large compact clusters will appear as rough nearly spherical objects to the mesoscopic solvent and on large enough scales the interactions with the solvent should be mimicked by stick boundary conditions at the cluster surfaces to the surrounding fluid with viscosity η. Consequently, in this large particle limit, one might expect the diffusion coefficient to be given approximately by the Stokes-Einstein relation: D_{SE} = kT/6$\pi\eta R_c$, where R_c is the radius of the cluster. From the site radial distribution function data (Figures 1 and 3) one may obtain crude estimates of the cluster size and we find $R_c \approx$ 15.7 and 18.1 A for *n*-heptane and *n*-decane clusters, respectively. The viscosities of the mesoscopic solvents for *n*-heptane cluster at 170 K calculated from the Stokes-Einstein relation using the diffusion data in Table 4 are 1.40, 1.65, 2.12, 3.39, and 4.55×10^{-4} N·s/m^2 for N=2000-32000. Those for *n*-decane cluster at 190 K are 1.86, 2.09, 2.44, 4.07, and 5.24×10^{-4} N · s/m^2 for N = 2,000-32,000.

The viscosity of the mesoscopic solvent for both *n*-alkane clusters increases with increasing N, and that for *n*-decane cluster for a given N is larger than that for *n*-heptane cluster for the same N since the excluded volume by the cluster molecules is larger. One can see that the values of $g_{CM-s}(r)$ for the *n*-decane cluster at large r^* in Figure 3 is greater than those for the *n*-heptane cluster in Figure 1.

Conclusion

In this paper we have presented the results of structural and dynamic properties of small *n*-alkane clusters embedded in a mesoscopic solvent using a hybrid molecular dynamics simulation in which solute molecules evolve by Newton's equations of motion but the solvent evolves through the multi-particle mesoscale dynamics. Some equilibrium properties for *n*-alkane clusters of M = 100 show a turnover point as a function of the number of the mesoscopic solvent molecules, N. For example, the C-C-C-C *trans* % increases with increasing N and then decreases when N is too large. The turnover seems to occur at N = 16,000 for the *n*-heptane cluster and at N = 8,000 for the *n*-decane cluster, respectively.

The site radial distribution function for *n*-heptane clusters of M = 100 in vacuum at T = 170 K shows liquid-like

Table 4. Self-diffusion constants (10^{-6} cm^2/sec) of the center of mass of *n*-heptane clusters at 170 K and *n*-decane clusters at 190 K in the mesoscopic solvents calculated from MSD's and VAC's. Uncertainties in the last reported digit are given in parenthesis

n-alkane clusters	N = 2,000		N = 4,000		N = 8,000		N = 16,000		N = 32,000	
	MSD	VAC	MSD	VAC	MSD	VAC	MSD	VAC	MSD	VAC
n-C_7H_{16}	5.65(14)	5.69(12)	4.80(10)	4.85(11)	3.74(13)	3.78(12)	2.34(10)	2.35(9)	1.74(4)	1.75(4)
n-$C_{10}H_{22}$	4.14(9)	4.17(10)	3.68(5)	3.72(7)	3.16(12)	3.17(14)	1.89(9)	1.90(10)	1.47(7)	1.49(8)

distributions of cluster particles and no structural ordering within the cluster. The modifications in the cluster structure occur when the clusters are embedded in the mesoscopic solvent. In the cases of N = 2,000 and 4,000 the structures of the radial distribution functions are similar to the corresponding vacuum structure. As N increases, prominent cluster particle layers become appeared and four prominent cluster particle layers are clearly seen when N = 16,000.

The diffusion coefficient of the center of mass for *n*-alkane cluster in the mesoscopic solvent decreases with increasing N. The viscosity of the mesoscopic solvent for both *n*-alkane clusters obtained from the Stokes-Einstein relation using the diffusion data is fully understood by the structure of the solvent molecule-cluster particle distributions.

Acknowledgment. This research was supported by Kyungsung University Research Grants in 2003. This research is a partial fulfillment of the requirements for the degree of Master of Education for SYK at Department of Chemistry, Graduate School of Education, Kyungsung University.

References

1. Chandrasekhar, S. *Rev. Mod. Phys.* **1943**, *15*, 1.
2. (a) Mareschal, M. *Microscopic Simulations of Complex Flows*; Plenum: New York, 1990. (b) Kong, Y.; Manke, C. W.; Madden, W. G.; Schlijper, A. G. *J. Chem. Phys.* **1997**, *107*, 592.
3. Ermak, D. L.; MaCammon, J. A. *J. Chem. Phys.* **1993**, *99*, 8016.
4. Bird, G. A. *Molecular Gas Dynamics*; Clarendon: Oxford, 1976.
5. For a review, see Chen, S.; Doolen, G. *Annu. Rev. Fluid Mech.* **1998**, *20*, 329.
6. Rothman, D. H.; Zaleski, S. *Lattice-Gas Cellular Automata: Simple Models of Complex Hydrodynamics*; Cambridge University Press: Cambridge, 1997.
7. Malevanets, A.; Kapral, R. *J. Chem. Phys.* **1999**, *110*, 8605.
8. Malevanets, A.; Kapral, R. *J. Chem. Phys.* **2000**, *112*, 7260.
9. Lee, S. H.; Kapral, R. *Physica A* **2001**, *298*, 56.
10. Mondello, M.; Grest, G. S. *J. Chem. Phys.* **1995**, *103*, 7156.
11. Mondello, M.; Grest, G. S. *J. Chem. Phys.* **1997**, *106*, 9327.
12. Mondello, M.; Grest, G. S.; Webb, E. B.; Peczak, P. *J. Chem. Phys.* **1998**, *109*, 798.
13. Siepmann, J. I.; Karaborni, S.; Smit, B. *Nature* (London) **1993**, *365*, 330.
14. Smit, B.; Karaborni, S.; Siepmann, J. I. *J. Chem. Phys.* **1995**, *102*, 2126.
15. Mundy, C. J.; Siepmann, J. I.; Klein, M. L. *J. Chem. Phys.* **1995**, *102*, 3376.
16. Cui, S. T.; Cummings, P. T.; Cochran, H. D. *J. Chem. Phys.* **1996**, *104*, 255.
17. Cui, S. T.; Gupta, S. A.; Cummings, P. T.; Cochran, H. D. *J. Chem. Phys.* **1996**, *105*, 1214.
18. Jorgensen, W. L.; Madura, J. D.; Swenson, C. J. *J. Am. Chem. Soc.* **1984**, *106*, 6638.
19. Allen, M. P.; Tildesley, D. J. *Computer Simulation of Liquids*; Oxford Univ. Press.: Oxford, 1987; p 81.
20. Andersen, H. *J. Comput. Phys.* **1984**, *52*, 24.
21. Evans, D. J.; Hoover, W. G.; Failor, B. H.; Moran, B.; Ladd, A. J. C. *Phys. Rev. A* **1983**, *28*, 1016.
22. Simmons, A. D.; Cummings, P. T. *Chem. Phys. Lett.* **1986**, *129*, 92.
23. Goldstein, H. *Classical Mechanics*; Addison-Wesley, Harvard University: 1974; p 155.
24. McQuarrie, D. A. *Statistical Mechanics*; Harper and Row: New York, 1976.